Solving a class of biological HIV infection model of latently infected cells using heuristic approach

Yolanda Guerrero Sanchez[1], Muhammad Umar[2, a], Zulqurnain Sabir[2, b], Juan L.G. Guirao[3, *], Muhammad Asif Zahoor Raja[4]

[1]Department of Dermatology, Stomatology, Radiology and Physical Medicine, University of Murcia, Spain

Email: yolanda.guerreros@um.es

[2]Department of Mathematics and Statistics, Hazara University, Mansehra, Pakistan

[a]Emails: umar_maths@hu.edu.pk, humar922015@gmail.com

[b]Emails: zulqurnain_maths@hu.edu.pk, zulqurnainsabir@gmail.com, +923335868270

[3]Department of Applied Mathematics and Statistics, Technical University of Cartagena, Hospital de Marina 30203-Cartagena, Spain

Email: juan.garcia@upct.es

*Corresponding author

[4]Department of Electrical and Computer Engineering, COMSATS University Islamabad, Attock Campus, Attock, Pakistan

Email: Muhammad.asif@ciit-attock.edu.pk

Abstract:

The intension of the recent study is to solve a class of biological nonlinear HIV infection model of latently infected CD4+T cells using feed-forward artificial neural networks, optimized with global search method, i.e. particle swarm optimization (PSO) and quick local search method, i.e. interior-point algorithms (IPA). An unsupervised error function is made based on the differential equations and initial conditions of the HIV infection model represented with latently infected CD4+T cells. For the correctness and reliability of the present scheme, comparison is made of the present results with the Adams numerical results. Moreover, statistical measures based on mean absolute deviation, Theil's inequality coefficient as well as root mean square error demonstrates the effectiveness, applicability and convergence of the designed scheme.

Keywords: HIV infection, particle swarm, hybrid approach, interior-point algorithm, artificial neural networks, statistical analysis.

Nomencleature

1. Introduction

HIV is known as a hazardous virus that grows by exploitation of body fluids and damage the immune system of the body. It destroys and kills many of the CD4 cells (T cells), so the body fails to fight off disease and infections, due to this, the CD4 cells are reduced. The attack on the immune system weakens the performance of the body to resist against infections and other diseases. Many serious/global diseases like cancer, HIV/AIDS and opportunistic infections get the advantage of the weak body's immune system. The huge amount has been spent for the treatment of these kinds of diseases every year, but no cure is found yet [1]. The research community has introduced

valuable mathematical formulations for understanding the dynamics of HIV infection spread and disease progression [2-6]. Research community shows that a substantial concentration of the T cells is effected via HIV virus attack and they presented a mathematical model of HIV infection spread in 1989 [7]. The main features of this model have three variables: infected, uninfected and virus free cells.

To present the HIV infection model, the infected CD4+ T-cells [7-8] are assumed in latent or active state. Due to infection, most of the healthy T-cells lost, however, a small proportion of said cells may be productively infected, i.e., in active or latent state. The mathematical model of HIV infection in simple terms is given as follows [9-10]:

$$\begin{cases} \dfrac{dx}{dt} = \mu - dx - \alpha xv, & x(0) = S_1, \\ \dfrac{dw}{dt} = -(q-1)\alpha xv - ew - \lambda w, & w(0) = S_2, \\ \dfrac{dy}{dt} = \lambda w - ay + q\alpha xv, & y(0) = S_3, \\ \dfrac{dv}{dt} = -uv + ky, & v(0) = S_4. \end{cases} \tag{1}$$

where x, w, y, and v stand for susceptible, infected, recover and latently infected CD4+T virus cells, with respective initial concentrations of S_1, S_2, S_3 and S_4, λ is a constants for recovery rate, α is the rate of infection, μ is the rate of iterance of uninfected CD4+T cells, d stands for rate of death for susceptible CD4+T cells, a is the death rate of HIV recover cells, e is the infection rate by recombination, k is the rate of latently infection HIV cells, u is the death rate of latently infected cells and q is the removal rate of recombinants.

To solve the biological model (1) is not easy due to the nonlinearity. However, only a few techniques are available in the literature to solve the biological nonlinear HIV infection model of latently infected CD4+T cells. Few of them are Adomian decomposition method [10], finite difference scheme [11], Legendre wavelet method [12], sequential Bayesian analysis approach [13], homotopy analysis method [14], Bessel collocation technique [15] and method of differential transformation [16].

All the above mention techniques have their individual merits/demerits, advantages/disadvantages, whereas, stochastic numerical solvers based on artificial neural networks (ANNs) are found to be efficient, precise and consistent for solving competently optimization models arising in various fields [17-21]. Some recent applications of stochastic solvers are nonlinear prey-predator models [22], nonlinear Troesch's problem arising in plasma physics [23], cell biology [24], inverse kinematics problems [25], thin-film flow [26], uncertainties in computational mechanics [27], power [28], fuzzy differential equations [29], nanofluidic problems [30], nonlinear singular Thomas-Fermi systems [31], doubly-singular systems [32], heat conduction model of human head [33], transistor-level uncertainty quantification [34], control system [35] and energy [36].

The aim of the present work is to solve the HIV model (1) numerically by using the ANNs optimized by particle swarm optimization (PSO), interior-point algorithm (IPA) and the hybrid combination of PSO-IPA. Some prime features of the present scheme are as follows:

- A novel development of ANNs based numerical computing method is presented to obtain the accurate and consistent approximate solutions for the nonlinear biological model of HIV infection spread.
- The presented approach is implemented viably to solve the nonlinear biological model and outcomes of the designed scheme are in good agreement with the Adams numerical results that endorsed its worth.
- Validation via statistics through reasonable accurate values of different performance metrics in terms of minimum, maximum, median and semi interquartile ranges.

2. Design Methodology

The proposed structure of the present scheme of the model (1) is divided into two portions. By introducing an error based fitness function and the combination of PSO-IPA along with the pseudocode is discussed in detail, while and the graphical abstract of PSO-IPA is plotted in Fig. 1.

2.1 ANN Modeling

The formulation of the model (1) with feed-forward ANNs in the form of $x(t), w(t), y(t)$ and v(t), as well as, their respective *n* derivatives are given as:

$$\begin{bmatrix} \hat{x}(t), \hat{w}(t), \\ \hat{y}(t), \hat{v}(t) \end{bmatrix} = \begin{bmatrix} \sum_{i=1}^{m} \varphi_{x,i} h(\phi_{x,i} t + b_{x,i}), \sum_{i=1}^{m} \varphi_{w,i} h(\phi_{w,i} t + b_{w,i}), \\ \sum_{i=1}^{m} \varphi_{y,i} h(\phi_{y,i} t + b_{y,i}), \sum_{i=1}^{m} \varphi_{v,i} h(\phi_{v,i} t + b_{v,i}) \end{bmatrix}, \tag{2}$$

$$\begin{bmatrix} \hat{x}^{(n)}, \hat{w}^{(n)}, \\ \hat{y}^{(n)}, \hat{v}^{(n)} \end{bmatrix} = \begin{bmatrix} \sum_{i=1}^{m} \varphi_{x,i} h^{(n)}(\phi_{x,i} t + b_{x,i}), \sum_{i=1}^{m} \varphi_{w,i} h^{(n)}(\phi_{w,i} t + b_{w,i}), \\ \sum_{i=1}^{m} \varphi_{y,i} h^{(n)}(\phi_{y,i} t + b_{y,i}), \sum_{i=1}^{m} \varphi_{v,i} h^{(n)}(\phi_{v,i} t + b_{v,i}) \end{bmatrix}.$$

Where $\boldsymbol{W}$ is the unknown weight vector and defined as:

$\boldsymbol{W} = [\boldsymbol{W}_x, \boldsymbol{W}_w, \boldsymbol{W}_y, \boldsymbol{W}_v]$, for $\boldsymbol{W}_x = [\boldsymbol{\varphi}_x, \boldsymbol{\phi}_x, \boldsymbol{b}_x]$, $\boldsymbol{W}_w = [\boldsymbol{\varphi}_w, \boldsymbol{\phi}_w, \boldsymbol{b}_w]$, $\boldsymbol{W}_y = [\boldsymbol{\varphi}_y, \boldsymbol{\phi}_y, \boldsymbol{b}_y]$ and $\boldsymbol{W}_v = [\boldsymbol{\varphi}_v, \boldsymbol{\phi}_v, \boldsymbol{b}_v]$. The weight vector $\boldsymbol{W}$ is given as:

$$\boldsymbol{\varphi}_x = [\varphi_{x,1}, \varphi_{x,2}, ..., \varphi_{x,m}], \boldsymbol{\varphi}_w = [\varphi_{w,1}, \varphi_{w,2}, ..., \varphi_{w,m}], \boldsymbol{\varphi}_y = [\varphi_{y,1}, \varphi_{y,2}, ..., \varphi_{y,m}], \boldsymbol{\varphi}_v = [\varphi_{v,1}, \varphi_{v,2}, ..., \varphi_{v,m}],$$
$$\boldsymbol{\phi}_x = [\phi_{x,1}, \phi_{x,2}, ..., \phi_{x,m}], \boldsymbol{\phi}_w = [\phi_{w,1}, \phi_{w,2}, ..., \phi_{w,m}], \boldsymbol{\phi}_y = [\phi_{y,1}, \phi_{y,2}, ..., \phi_{y,m}], \boldsymbol{\phi}_v = [\phi_{v,1}, \phi_{v,2}, ..., \phi_{v,m}],$$
$$\boldsymbol{b}_x = [b_{x,1}, b_{x,2}, ..., b_{x,m}], \boldsymbol{b}_w = [b_{w,1}, b_{w,2}, ..., b_{w,m}], \boldsymbol{b}_y = [b_{y,1}, b_{y,2}, ..., b_{y,m}], \boldsymbol{b}_v = [b_{v,1}, b_{v,2}, b_{v,3}, ..., b_{v,m}].$$

Using the log-sigmoid activation function $\frac{1}{1+\exp(-t)}$. The updated form of the network (2) becomes as:

$$\begin{bmatrix} \hat{x}(t), \hat{w}(t), \\ \hat{y}(t), \hat{v}(t) \end{bmatrix} = \begin{bmatrix} \sum_{i=1}^{m} \frac{\varphi_{x,i}}{1+e^{-\left(\phi_{x,i}t+b_{x,i}\right)}}, \sum_{i=1}^{m} \frac{\varphi_{w,i}}{1+e^{-\left(\phi_{w,i}t+b_{w,i}\right)}}, \\ \sum_{i=1}^{m} \frac{\varphi_{y,i}}{1+e^{-\left(\phi_{y,i}t+b_{y,i}\right)}}, \sum_{i=1}^{m} \frac{\varphi_{v,i}}{1+e^{-\left(\phi_{v,i}t+b_{v,i}\right)}} \end{bmatrix},$$

$$\begin{bmatrix} \hat{x}'(t), \hat{w}'(t), \\ \hat{y}'(t), \hat{v}'(t) \end{bmatrix} = \begin{bmatrix} \sum_{i=1}^{m} \frac{\varphi_{x,i}\phi_{x,i}e^{-\left(\phi_{x,i}t+b_{x,i}\right)}}{\left(1+e^{-\left(\phi_{x,i}t+b_{x,i}\right)}\right)^2}, \sum_{i=1}^{m} \frac{\varphi_{w,i}\phi_{w,i}e^{-\left(\phi_{w,i}t+b_{w,i}\right)}}{\left(1+e^{-\left(\phi_{w,i}t+b_{w,i}\right)}\right)^2}, \\ \sum_{i=1}^{m} \frac{\varphi_{y,i}\phi_{y,i}e^{-\left(\phi_{y,i}t+b_{y,i}\right)}}{\left(1+e^{-\left(\phi_{y,i}t+b_{y,i}\right)}\right)^2}, \sum_{i=1}^{m} \frac{\varphi_{v,i}\phi_{w,i}e^{-\left(w_{v,i}t+b_{v,i}\right)}}{\left(1+e^{-\left(\phi_{v,i}t+b_{v,i}\right)}\right)^2} \end{bmatrix}. \quad \textbf{(3)}$$

Using the model (3), the fitness/error function is written as:

$$\xi = \xi_1 + \xi_2 + \xi_3 + \xi_4 + \xi_5, \quad \textbf{(4)}$$

$$\xi_1 = \frac{1}{N}\sum_{m=1}^{N}\left(\frac{dx_m}{dt} - \mu + dx_m + \alpha x_m v_m\right)^2, \quad \textbf{(5)}$$

$$\xi_2 = \frac{1}{N}\sum_{m=1}^{N}\left(\frac{dw_m}{dt} + (q-1)\alpha x_m v_m + e w_m + \lambda w_m\right)^2, \quad \textbf{(6)}$$

$$\xi_3 = \frac{1}{N}\sum_{m=1}^{N}\left(\frac{dy_m}{dt} - \lambda w_m + a y_m - q\alpha x_m v_m\right)^2, \quad \textbf{(7)}$$

$$\xi_4 = \frac{1}{N}\sum_{m=1}^{N}\left(\frac{dv_m}{dt} + u v_m - k y_m\right)^2, \quad \textbf{(8)}$$

$$\xi_5 = \frac{1}{3}\left(\left(\hat{x}_0 - S_1\right)^2 + \left(\hat{w}_0 - S_2\right)^2 + \left(\hat{y}_0 - S_3\right)^2 + \left(\hat{v}_0 - S_4\right)^2\right), \quad \textbf{(9)}$$

for $N = \frac{1}{h}$, $\hat{x}_m = \hat{x}(t_m)$, $\hat{w}_m = \hat{w}(t_m)$, $\hat{y}_m = \hat{y}(t_m)$, $\hat{v}_m = \hat{v}(t_m)$, $t_m = mh$, $\hat{x}_m$, $\hat{w}_m$, $\hat{y}_m$, and $\hat{v}_m$ are representing the approximate solution for susceptible, *x*, infected *w*, recovered *y*, and latently infected *v* CD4+T virus cells for the m_{th} input grid point, respectively. Accordingly, ξ_1, ξ_2, ξ_3 and ξ_4 are the fitness functions associated with differential equations of the model (1) for susceptible, *x*, infected *w*, recovered *y*, and latently infected *v* CD4+T virus cells, respectively. while, ξ_5 is the error function related to the initial condition of model (1). The proposed approximate solution can be attained from the available weights for which the fitness function in equation (4) approaches to zero, i.e., $\xi \to 0$. Then the approximate solutions $\left[\hat{x}(t), \hat{w}(t), \hat{y}(t), \hat{v}(t)\right]$

become identical with exact/desire results, *i.e.*, $[\hat{x}(t) \to x(t)]$, $[\hat{w}(t) \to w(t)]$, $[\hat{y}(t) \to y(t)]$ and $[\hat{v}(t) \to v(t)]$.

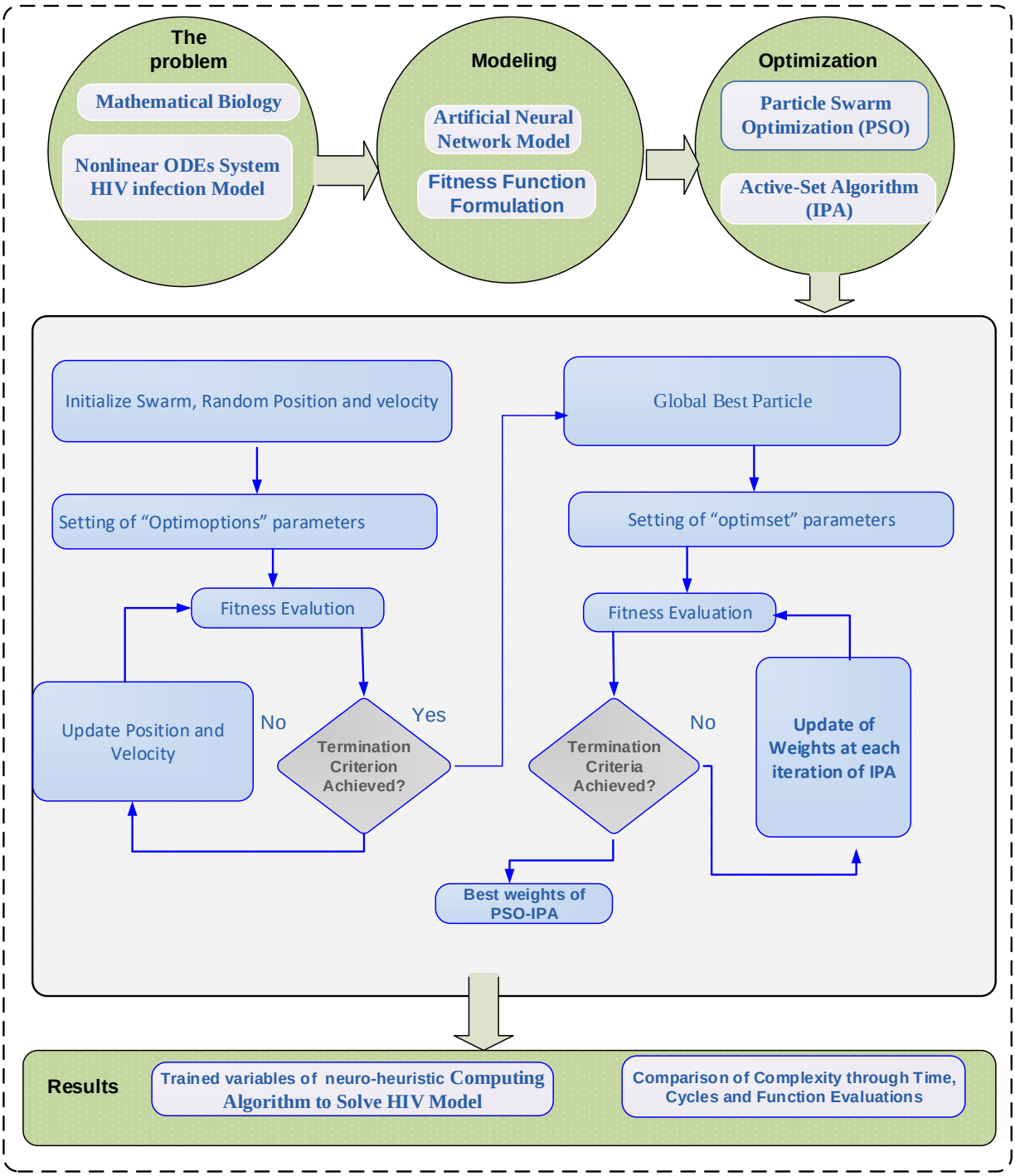

Figure 1: Graphical illustration of presented scheme for HIV infection model of latently infected cells

2.2. Optimization procedure: PSO-IPA

For optimization of ANNs, hybrid-computing framework based on PSO-IPA is used.

The PSO is a kind of effective global search heuristics method for optimization, suggested by Eberhart and Kennedy [37] and exploited by the research community as a replacement of genetic algorithms (GAs). The PSO is used as an optimization procedure because of easy implementation and short memory requirements [38-39]. Few recent potential applications addressed by PSO include fuel ignition model [40], solar photovoltaic system [41] and clustering high-dimensional data [42]. Therefore, PSO based algorithm should be testing for analysis of still nonlinear systems represented with differential equations [43-47].

In the theory of search space, every single candidate solution is denoted as a particle, and set of particles formulate a swarm. The position and velocity in the swarm are denoted by $\boldsymbol{P}_{LB}^{a-1}$ and $\boldsymbol{P}_{GB}^{a-1}$, respectively. The optimization model of PSO in standard mathematical notation is presented as follows:

$$\boldsymbol{X}_j^a = \boldsymbol{X}_j^{a-1} + \boldsymbol{V}_j^{a-1}, \tag{10}$$

$$\boldsymbol{V}_j^a = \omega \boldsymbol{V}_j^{a-1} + a_1 \boldsymbol{r}_1 (\boldsymbol{P}_{LB}^{a-1} - \boldsymbol{X}_j^{a-1}) + a_2 \boldsymbol{r}_2 (\boldsymbol{P}_{GB}^{a-1} - \boldsymbol{X}_j^{a-1}), \tag{11}$$

where the vector $\mathbf{X}_j$ and $\boldsymbol{V}_j$ represents the j_{th} particle of the swarm and associated velocity vector, respectively. The random vectors are $\boldsymbol{r}_1$ and $\boldsymbol{r}_2$, ω is the inertia weight of previous velocity, whereas, a_1 and a_2 are the local and global acceleration factors, respectively. The superscript α is the flight index. The performance of global search with PSO is further enhanced with the help of Interior-point algorithm, i.e., an efficient, rapid and fast local search optimization algorithm. Few IPA equally effective for both constrained and unconstrained optimization tasks. Recently, IPA is exploited in many fields e.g., active noise control problems [48], simulation of aircraft parts riveting [49], simulation of viscoplastic fluid flows [50], reliable treatment of economic load dispatch problem [51], for non-smooth contact dynamics [52] and non-smooth contact dynamics. In the proposed study, a hybrid computing tool PSO-IPA is exploited to tune the decision variables of ANN representing the model (1). The pseudocode of PSO-IPA is presented in Table 1.

3. Performance indices

The performance measures for the HIV model (1) based on mean absolute deviation (MAD), root mean square error (RMSE) and Theil's inequality coefficient (TIC). The mathematical form of MAD, RMSE and TIC is given as:

$$\left[MAD_x, MAD_w, MAD_y, MAD_v\right] = \begin{bmatrix} \frac{1}{m}\sum_{i=1}^{m}\left|x_i - \hat{x}_i\right|, \frac{1}{m}\sum_{i=1}^{m}\left|w_i - \hat{w}_i\right|, \\ \frac{1}{m}\sum_{i=1}^{m}\left|y_i - \hat{y}_i\right|, \frac{1}{m}\sum_{i=1}^{m}\left|v_i - \hat{v}_i\right| \end{bmatrix}, \tag{12}$$

$$[\mathrm{RMSE}_x,\mathrm{RMSE}_w,\mathrm{RMSE}_y,\mathrm{RMSE}_v]=\begin{bmatrix}\sqrt{\frac{1}{m}\sum_{i=1}^{m}(x_i-\hat{x}_i)^2},\sqrt{\frac{1}{m}\sum_{i=1}^{m}(w_i-\hat{w}_i)^2}\\ \sqrt{\frac{1}{m}\sum_{i=1}^{m}(y_i-\hat{y}_i)^2},\sqrt{\frac{1}{m}\sum_{i=1}^{m}(v_i-\hat{v}_i)^2}\end{bmatrix}., \quad \textbf{(13)}$$

$$[\mathrm{TIC}_x,\mathrm{TIC}_w,\mathrm{TIC}_y,\mathrm{TIC}_v]=\begin{pmatrix}\frac{\sqrt{\frac{1}{m}\sum_{i=1}^{m}(x_i-\hat{x}_i)^2}}{\left(\sqrt{\frac{1}{m}\sum_{i=1}^{m}x_i^2}+\sqrt{\frac{1}{m}\sum_{i=1}^{m}\hat{x}_i^2}\right)},\frac{\sqrt{\frac{1}{m}\sum_{i=1}^{m}(w_i-\hat{w}_i)^2}}{\left(\sqrt{\frac{1}{m}\sum_{i=1}^{m}w_i^2}+\sqrt{\frac{1}{m}\sum_{i=1}^{m}\hat{w}_i^2}\right)},\\ \frac{\sqrt{\frac{1}{m}\sum_{i=1}^{m}(y_i-\hat{y}_i)^2}}{\left(\sqrt{\frac{1}{m}\sum_{i=1}^{m}y_i^2}+\sqrt{\frac{1}{m}\sum_{i=1}^{m}\hat{y}_i^2}\right)},\frac{\sqrt{\frac{1}{m}\sum_{i=1}^{m}(v_i-\hat{v}_i)^2}}{\left(\sqrt{\frac{1}{m}\sum_{i=1}^{m}v_i^2}+\sqrt{\frac{1}{m}\sum_{i=1}^{m}\hat{v}_i^2}\right)}\end{pmatrix}. \quad \textbf{(14)}$$

Table 1: Pseudo code using PSO-IPA

Start of PSO

Inputs:

The chromosome with same number of entries of the network

$$\boldsymbol{W}=[\boldsymbol{W}_x,\boldsymbol{W}_w,\boldsymbol{W}_y,\boldsymbol{W}_v]=[(\boldsymbol{\varphi}_x,\boldsymbol{\phi}_x,\boldsymbol{b}_x),(\boldsymbol{\varphi}_w,\boldsymbol{\phi}_w,\boldsymbol{b}_w),(\boldsymbol{\varphi}_y,\boldsymbol{\phi}_y,\boldsymbol{b}_y),(\boldsymbol{\varphi}_v,\boldsymbol{\phi}_v,\boldsymbol{b}_v)]$$

$$\boldsymbol{\varphi}_x=[\varphi_{x,1},\varphi_{x,2},...,\varphi_{x,m}],\boldsymbol{\varphi}_w=[\varphi_{w,1},\varphi_{w,2},...,\varphi_{w,m}],\boldsymbol{\varphi}_y=[\varphi_{y,1},\varphi_{y,2},...,\varphi_{y,m}],\boldsymbol{\varphi}_v=[\varphi_{v,1},\varphi_{v,2},...,\varphi_{v,m}],$$

$$\boldsymbol{\phi}_x=[\phi_{x,1},\phi_{x,2},...,\phi_{x,m}],\boldsymbol{\phi}_w=[\phi_{w,1},\phi_{w,2},...,\phi_{w,m}],\boldsymbol{\phi}_y=[\phi_{y,1},\phi_{y,2},...,\phi_{y,m}],\boldsymbol{\phi}_v=[\phi_{v,1},\phi_{v,2},...,\phi_{v,m}],$$

$$\boldsymbol{b}_x=[b_{x,1},b_{x,2},...,b_{x,m}],\boldsymbol{b}_w=[b_{w,1},b_{w,2},...,b_{w,m}],\boldsymbol{b}_y=[b_{y,1},b_{y,2},...,b_{y,m}],\boldsymbol{b}_v=[b_{v,1},b_{v,2},b_{v,3},...,b_{v,m}].$$

Population: The set of chromosomes is

$$\boldsymbol{P}=[(\boldsymbol{W}_{x1},\boldsymbol{W}_{x2},...,\boldsymbol{W}_{xn}),(\boldsymbol{W}_{w1},\boldsymbol{W}_{w2},...,\boldsymbol{W}_{wn}),(\boldsymbol{W}_{y1},\boldsymbol{W}_{y2},...,\boldsymbol{W}_{yn}),(\boldsymbol{W}_{v1},\boldsymbol{W}_{v2},...,\boldsymbol{W}_{vn})]$$

$$[\boldsymbol{W}_{xi},\boldsymbol{W}_{wi},\boldsymbol{W}_{yi},\boldsymbol{W}_{vi}]=[(\boldsymbol{\varphi}_{xi},\boldsymbol{\phi}_{xi},\boldsymbol{b}_{xi}),(\boldsymbol{\varphi}_{wi},\boldsymbol{\phi}_{wi},\boldsymbol{b}_{wi}),(\boldsymbol{\varphi}_{yi},\boldsymbol{\phi}_{yi},\boldsymbol{b}_{yi}),(\boldsymbol{\varphi}_{vi},\boldsymbol{\phi}_{vi},\boldsymbol{b}_{vi})]$$

Output: Global best values of PSO is denoted as $\boldsymbol{W}_{\mathrm{B:PSO}}$

Initialization

Produce $\boldsymbol{W}$ of real numbers to signify a chromosome to make an Initial $\boldsymbol{P}$. Set the practice of Generation and declarations values of "PSO" and "gaoptimset" measures

Calculations of Fitness

To calculate the fitness ζ using Eq.(4)

Ranking

Each $\boldsymbol{W}$ of $\boldsymbol{P}$ ranked through brilliance of the fitness rate.

Stopping criteria

Stop the optimization procedure for any of the following

- Level of fitness achieved
- Number of preferred flights/cycles performed

Renewal

Call the position using equations (10) and velocity using equation (11).

Improvement

Repeat the algorithm until the whole number of flights achieved

Storage

Store the best fitness values and signify it the global best particle.

End of PSO algorithms

PSO-IPA Procedure Start

Inputs

$W_{B:GA}$

Output

The best vector of PSO:IPA is $W_{PSO:IPA}$

Initialize

Use $W_{B:GA}$ as a start point
Decelerations and bounded based on "optimset" and "fmincon" routines,

Termination

When any of the value meet, stop the algorithm
'Fitness limit' = '$\zeta \leq 10^{-18}$', 'total Iterations' = '1000', 'TolFun' ≤ '10^{-18}', 'TolX' ≤ '10^{-18}', 'TolCon' ≤ '10^{-20}', 'MaxFunEvals' ≤ '250000'

While (Terminate)

Fitness calculation

Using Eqs (4-9), find the fitness ζ

Adjustments

Invoking 'fmincon' routine using algorithm 'IPA' to adjust W.
Go to the step of fitness with updated W

End

Save the final adaptive weights $W_{PSO-:IPA}$ *and* ζ, iterations, time and function count for the current run.

PSO-IPA Procedure End

3. Results and discussion

The detailed result and discussion of the model (1) is presented in this section by taking five number of neurons. The comparative study with the Adams numerical results is also presented to show the exactness and correctness of the proposed scheme. Moreover, statistical results are performed to check the precision and accuracy of the present technique.

3.1 HIV infection model involving latently infected cells

The updated form of the model (1) by taking the values reported in the literature for HIV infection [10] as listed in Table 2

Table 2: List of parameter and setting used for reported study of HIV infection model

Index	Description	Settings [10]
S_1	Initial value of uninfected CD4+T cells	7
S_2	Initial value of infected CD4+T cells	2
S_3	Initial value of Virus free cells	1
S_4	Initial value of latently infected cells	4
μ	Rate of uninfected CD4+T cells	0.4
λ	Recovery Rate of infected cells	0.3
d	Death rate of uninfected CD4+T cells	0.01
α	Rate of infection spread	0.04
q	Rate of removal of recombinants	0.8
e	Rate of infection of recombinants	0.1
a	Death rate of virus free cells	0.2
u	Death rate of latently infected cells	0.03

The using the parameters as defined in Table 2, the model (1) is written in updated form as follows:

$$\begin{cases} \dfrac{dx}{dt} = 0.4 - 0.01x - 0.04xv, & x(0) = 7 \\ \dfrac{dw}{dt} = 0.008xv - 0.4w, & w(0) = 2 \\ \dfrac{dy}{dt} = 0.3w - 0.2y + 0.032xv, & y(0) = 1 \\ \dfrac{dv}{dt} = -0.03v + 0.6y, & v(0) = 4 \end{cases} \tag{15}$$

The error/fitness function of the model (15) is written as:

$$\begin{aligned} \zeta = \frac{1}{N}\sum_{m=1}^{N} & \left(\left[\frac{dx_m}{dt} - 0.4 + 0.01 * x_m + 0.04 * x_m v_m \right]^2 + \left[\frac{dw_m}{dt} - 0.008 * x_m v_m + 0.4 * v_m \right]^2 \right. \\ & \left. + \left[\frac{dy_m}{dt} - 0.3 * w_m + 0.2 * y_m - 0.032 * x_m * v_m \right]^2 + \left[\frac{dv_m}{dt} + v_m - 0.6 * y_m \right]^2 \right) \\ & + \frac{1}{4}\left(\left(\hat{x}_0 - 7\right)^2 + \left(\hat{w}_0 - 2\right)^2 + \left(\hat{y}_0 - 1\right)^2 + \left(\hat{v}_0 - 1\right)^2 \right), \end{aligned} \tag{16}$$

Optimization of all variants of the model (1) is supported by the combination of PSO-IPA for hundred numbers of runs to achieve the network parameters. The weights set is provided to obtain the approximate solution for the model (1). The mathematical form of the approximate solution becomes as:

$$\hat{x}(t) = \frac{0.1615}{1+e^{-(-4.5041t-2.7123)}} + \frac{1.4934}{1+e^{-(-1.3373t-0.5227)}} + \frac{6.8018}{1+e^{-(-3.0218t+6.9131)}} + \frac{-0.3605}{1+e^{-(0.2689t-1.1503)}} + \frac{-2.6949}{1+e^{-(1.1514t-2.1777)}}, \quad \textbf{(17)}$$

$$\hat{w}(t) = \frac{1.1743}{1+e^{-(-0.4197t-0.9589)}} + \frac{2.3207}{1+e^{-(-0.8906t-2.1978)}} + \frac{0.6713}{1+e^{-(-1.7834t-8.4626)}} + \frac{5.8251}{1+e^{-(0.0674t+1.0848)}} + \frac{-3.9497}{1+e^{-(0.4770t+1.0307)}}, \quad \textbf{(18)}$$

$$\hat{y}(t) = \frac{6.1731}{1+e^{-(0.4578t-3.9406)}} + \frac{4.0619}{1+e^{-(1.3612t+1.8178)}} + \frac{0.1770}{1+e^{-(0.5817t-0.6665)}} + \frac{-3.5977}{1+e^{-(-0.8200t+1.0544)}} + \frac{-0.1097}{1+e^{-(2.4635t-3.2401)}}, \quad \textbf{(19)}$$

$$\hat{v}(t) = \frac{1.5157}{1+e^{-(-1.0591t-5.8109)}} + \frac{-0.3853}{1+e^{-(-2.7099t+1.5490)}} + \frac{6.7429}{1+e^{-(0.0742t+0.1897)}} + \frac{5.6749}{1+e^{-(0.9777t-2.1071)}} + \frac{0.5811}{1+e^{-(-3.2119t-4.3057)}}. \quad \textbf{(20)}$$

The graphic illustration using GA-IPA for all the parameters of example 1 is narrated in Figures 2-7 in case of 5 neurons in ANN models. The set of weights for the parameters $x(t)$, $w(t)$, $y(t)$ and $v(t)$ using the best fitness values for 5 number of neuron is shown in Fig 2. The outcomes of proposed method ANN-PSO-IPA are presented in Fig. 3. The absolute error (AE) is calculated for the parameters $x(t)$ and $w(t)$ in the first half of Fig. 4, while the AE for $y(t)$ and $v(t)$ is calculated in the second half of Fig. 4. The presented results are compared with the Adams method based numerical results. It is clear in Fig. 4(a), that the AE for $x(t)$ and $w(t)$ lie in the ranges of 10^{-06} to 10^{-07}, while the AE for $y(t)$ and $v(t)$ lie around 10^{-05} to 10^{-07}. In these figures, the comparison with standard numerical results using 5 number of neurons in ANN models are provided. The first portion of the Fig. 4 shows the comparison for $x(t)$ and $w(t)$, while the second portion related the values of y(t) and $v(t)$. The overlapping of the present results with the Adams numerical results show the correctness and exactness of the present scheme. The performance measures along with the histograms of the statistical operators MAD, RMSE and TIC are narrated in Figs. 5 to 7. One may infer from results presented in these graphical illustration 80% or more of independent runs achieved the reasonable precise level of the statistical indices of MAD and RMSE. However, the level increasing up to 90% in case of TIC metric.

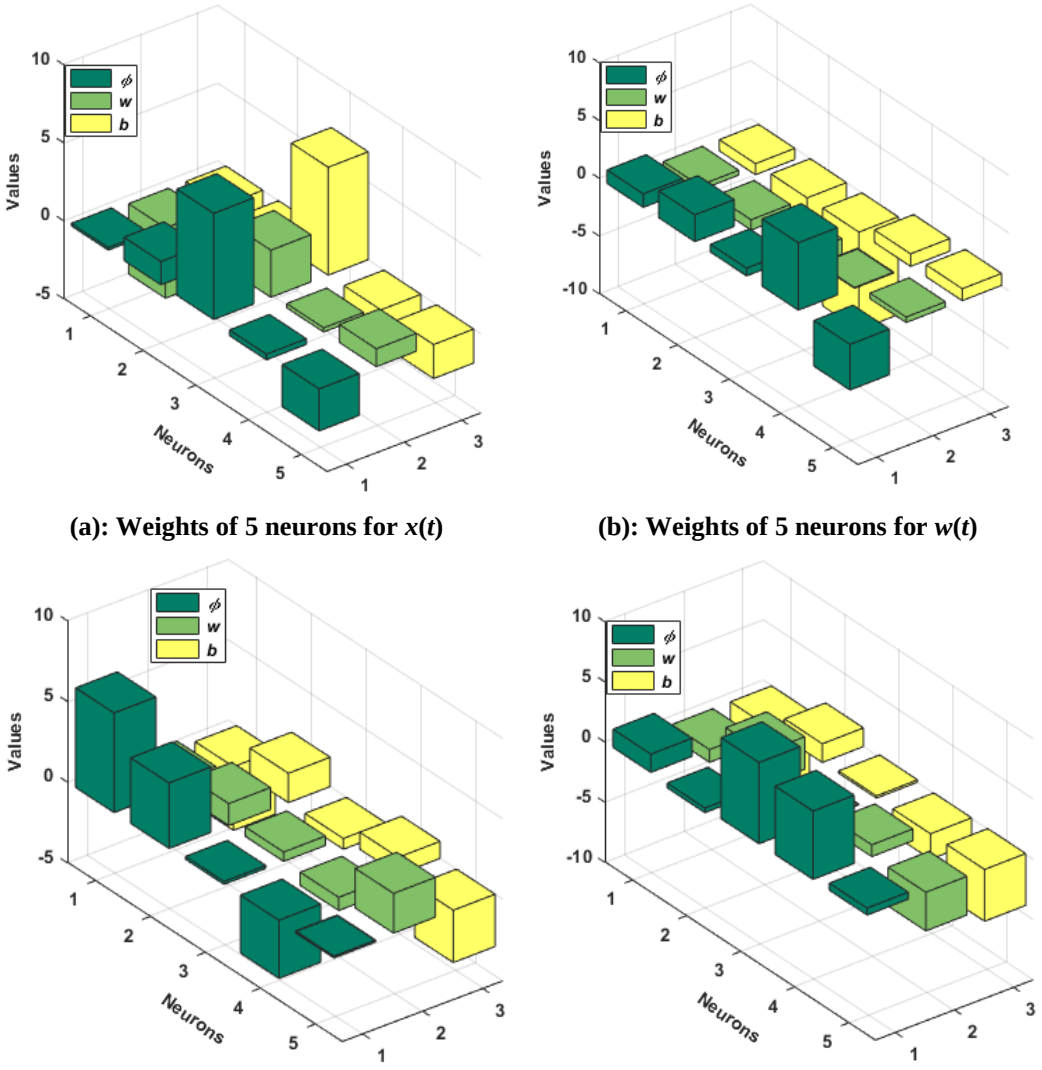

(a): Weights of 5 neurons for $x(t)$ **(b): Weights of 5 neurons for $w(t)$**

(c): Weights of 5 neurons for $y(t)$ **(d): Weights of 5 neurons for $v(t)$**

Figure 2: Trained weights or decision variables of ANN on the basis of best fitness achieved

For precision analysis, statistical gages based on minimum (Min), Maximum (Max), median (Med) and semi interquartile range (SIR) are provided for the present technique. SIR is one-half of the difference of third quartile (Q_3=75% data) and first quartile (Q_1= 25% data). The statistical conclusions in Min, Max, Med and SIR gages for problem 1 are tabulated in Tables 3 for $x(t)$ and $w(t)$, while in Table 4 for $y(t)$ and $v(t)$. The scale of Min values for $x(t)$, $w(t)$, $y(t)$ and $v(t)$ lies around 10^{-07} to 10^{-09} for all neurons. However, the Med and SIR values for $x(t)$, $w(t)$, $y(t)$ and $v(t)$ are closer to 10^{-05}.

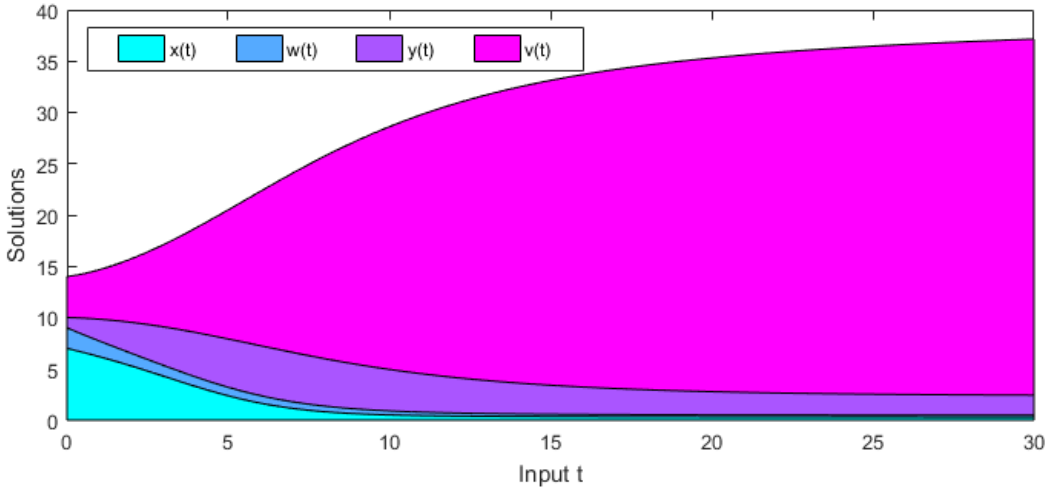

(a): Dynamics of HIV infection model

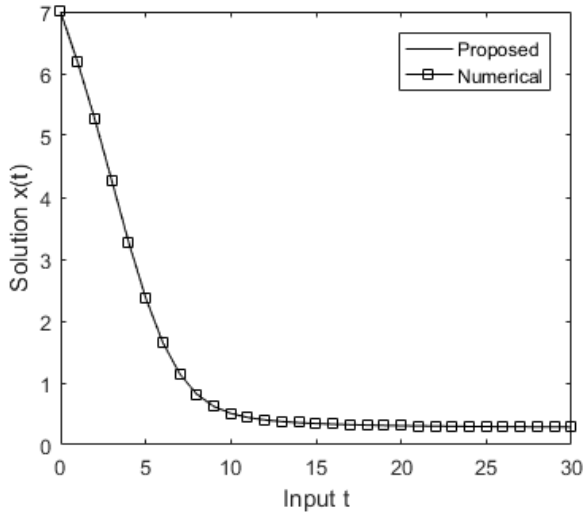

(b): Variation of x(t)

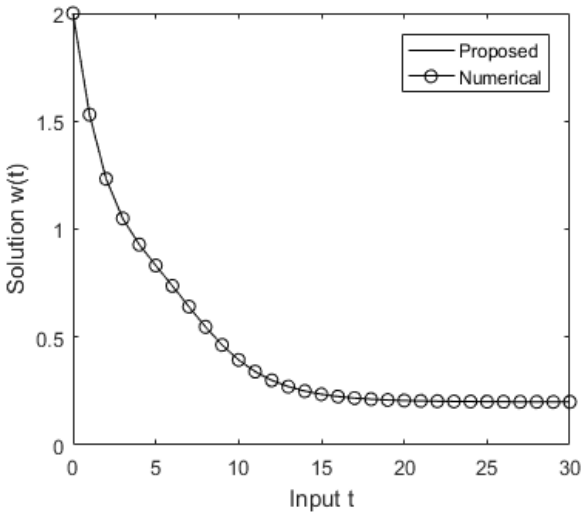

(c): Variation of w(t)

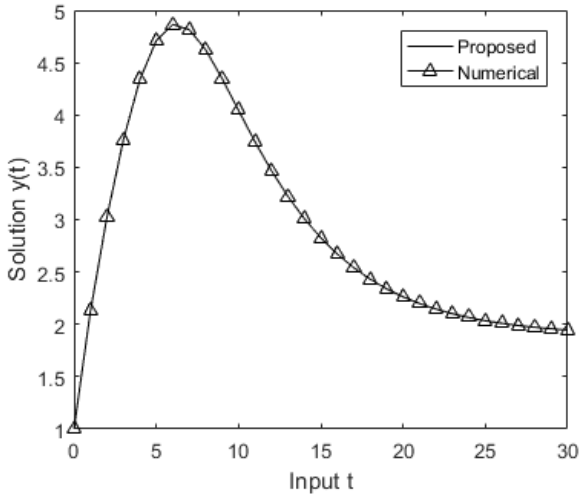

(d): Variation of y(t)

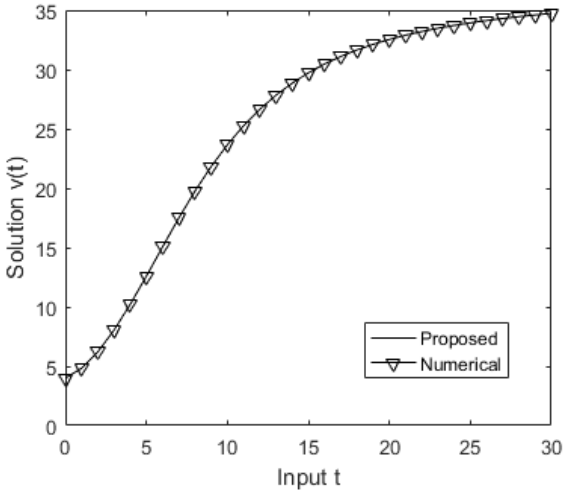

(e): Variation of v(t)

Figure 3: Results for HIV infection spread model

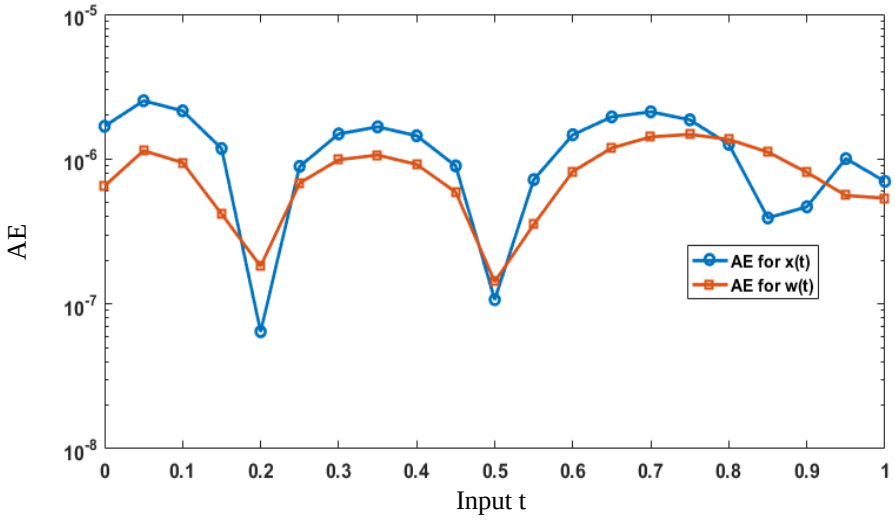

(a): Results on AE for 5 number of neurons in case of x(t) and w(t)

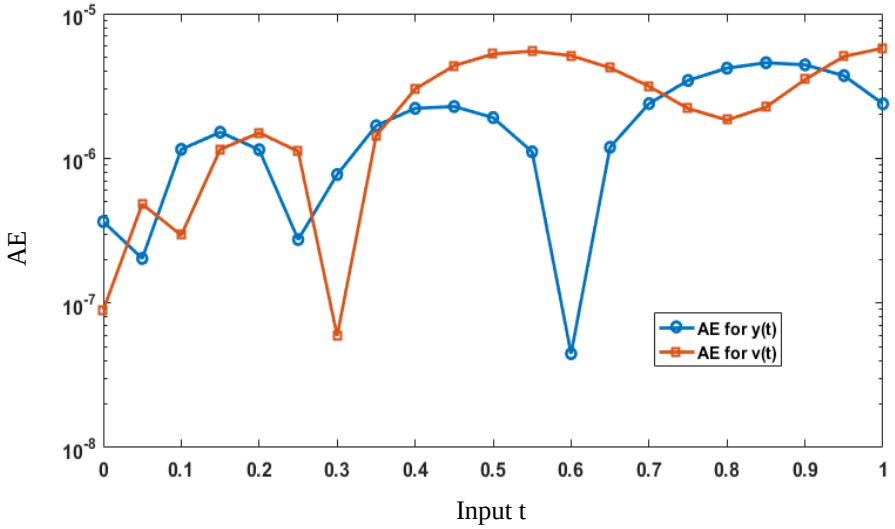

(b): Results on AE for 5 number of neurons in case of y(t) and v(t)

Figure 4: Comparative study on AE of the presented solutions using 5 neurons with the Adams results

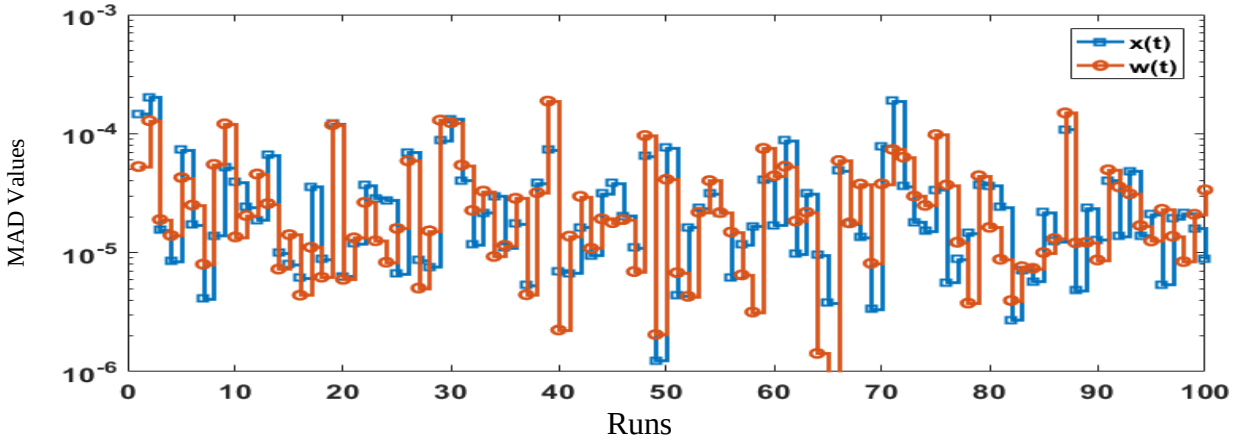

(a) Convergence analysis on MAD for $x(t)$ and $w(t)$

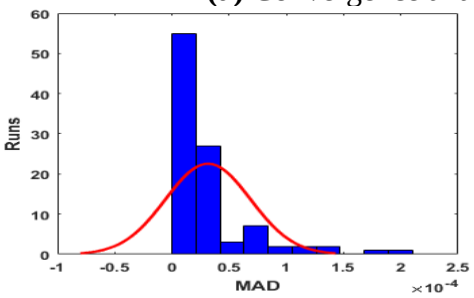

(a): Histogram for $x(t)$

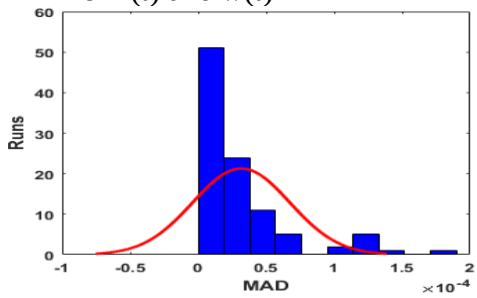

(c): Histogram for $w(t)$

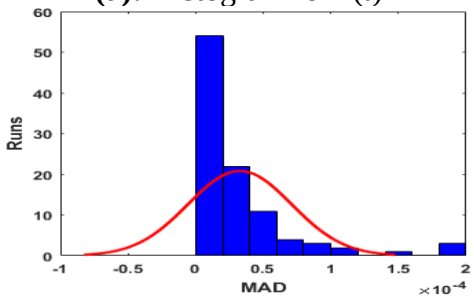

(c): Histogram for $y(t)$

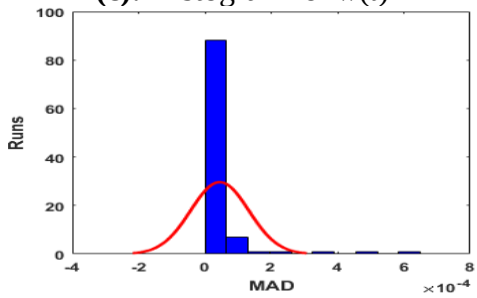

(d): Histogram for $v(t)$

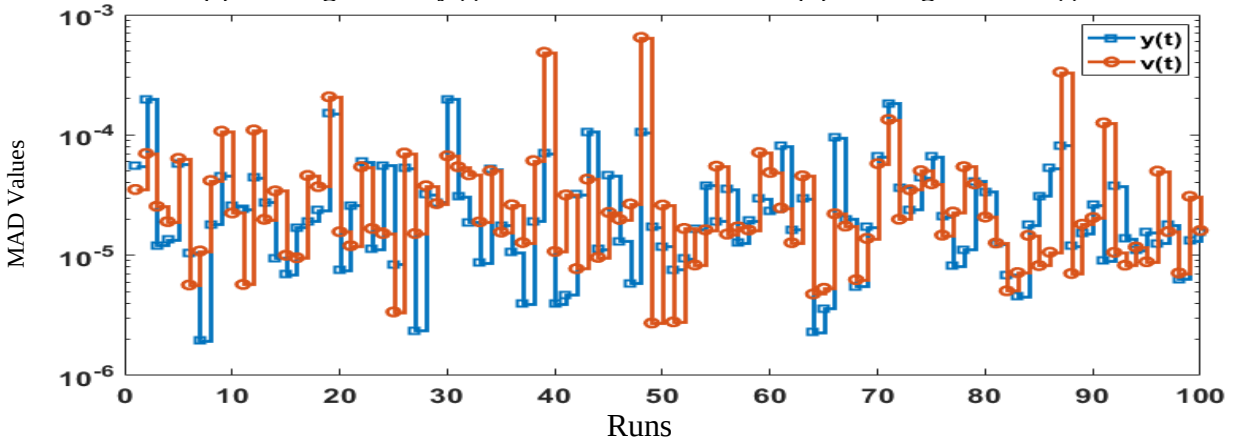

(a) Convergence analysis on MAD for $x(t)$ and $w(t)$

Figure 5: Analysis on MAD for convergence along with the histograms for 5 neurons

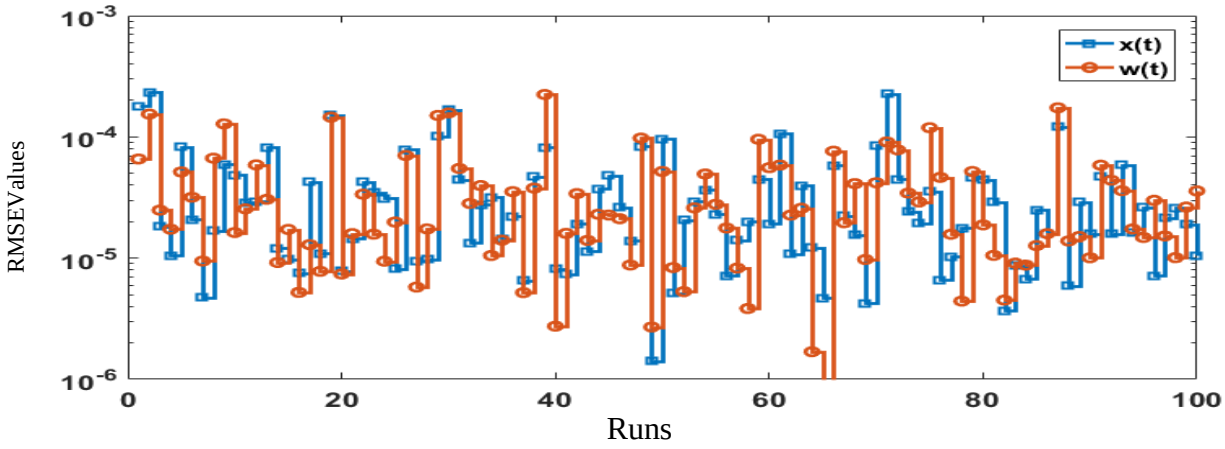

(a) Convergence analysis on RMSE for $x(t)$ and $w(t)$

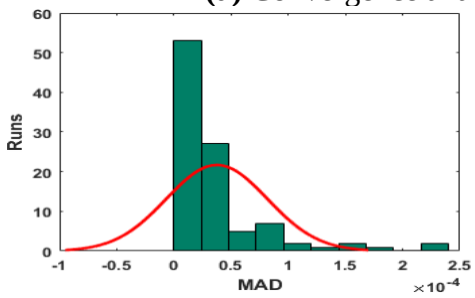

(a): Histogram for $x(t)$

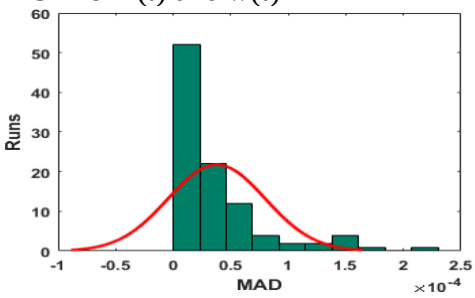

(c): Histogram for $w(t)$

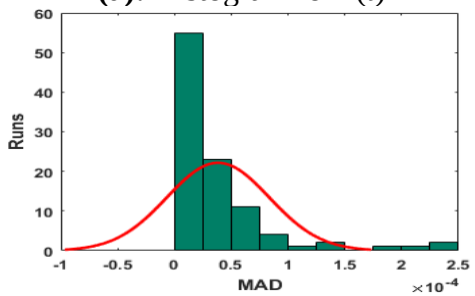

(c): Histogram for $y(t)$

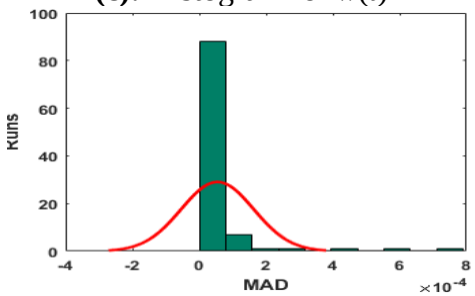

(d): Histogram for $v(t)$

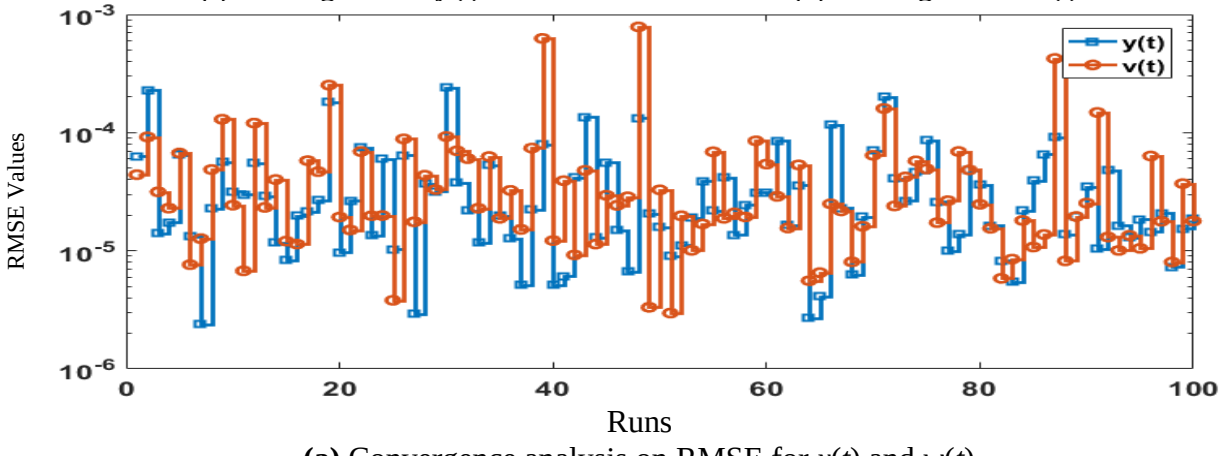

(a) Convergence analysis on RMSE for $x(t)$ and $w(t)$

Figure 6: Analysis on RMSE for convergence along with the histograms for 5 neurons

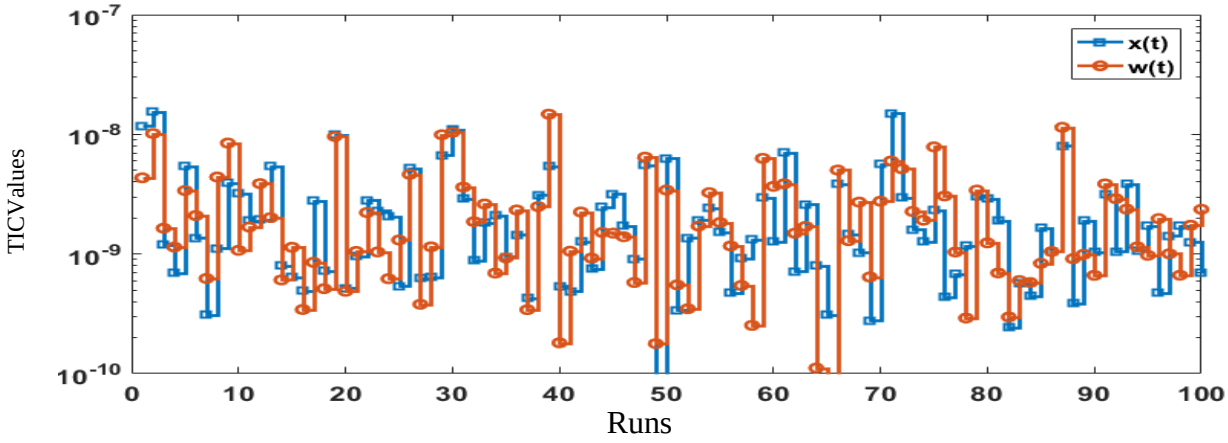

(a) Convergence analysis on RMSE for $x(t)$ and $w(t)$

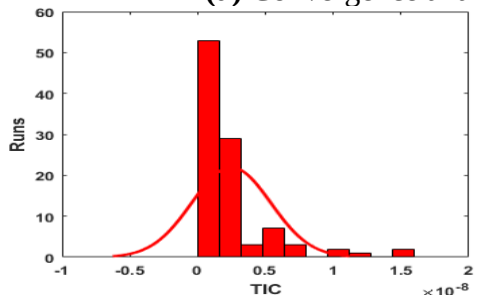

(a): Histogram for $x(t)$

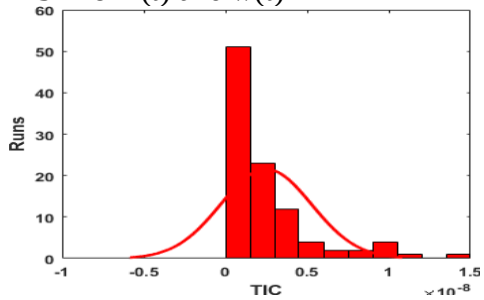

(c): Histogram for $w(t)$

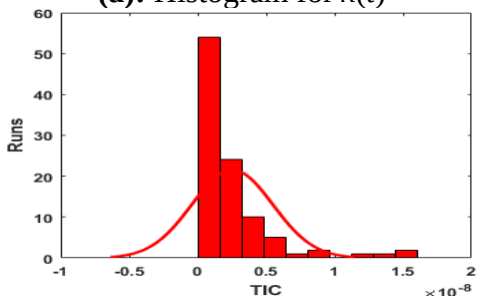

(c): Histogram for $y(t)$

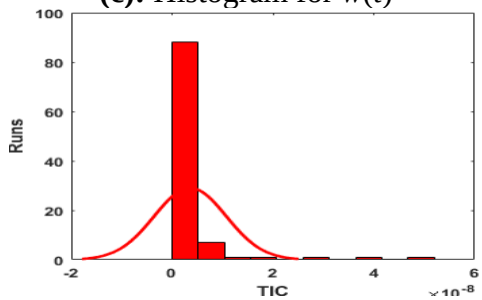

(d): Histogram for $v(t)$

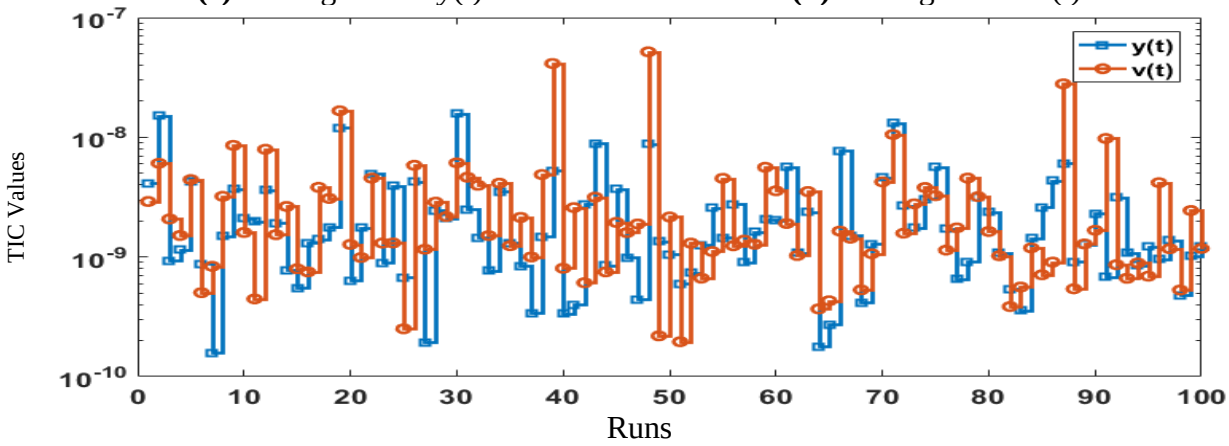

(a) Convergence analysis on RMSE for $x(t)$ and $w(t)$

Figure 7: Analysis on TIC for convergence along with the histograms for 5 neurons

Table 3: Statistics based results of Problems 1 for $x(t)$ and $w(t)$

t	$x(t)$				$w(t)$			
	Min	**Max**	**Med**	**SIR**	**Min**	**Max**	**Med**	**SIR**
0	1.998E-08	1.301E-04	4.388E-06	6.397E-06	3.113E-09	1.301E-04	4.174E-06	6.611E-06
0.05	8.551E-08	1.589E-04	1.004E-05	1.259E-05	3.198E-08	1.589E-04	1.194E-05	1.105E-05
0.1	4.509E-08	2.279E-04	1.028E-05	1.091E-05	2.524E-07	2.279E-04	1.370E-05	1.140E-05
0.15	4.956E-08	2.215E-04	1.250E-05	1.275E-05	2.549E-07	2.215E-04	1.146E-05	9.729E-06
0.2	6.438E-08	1.616E-04	1.741E-05	1.377E-05	8.992E-08	1.616E-04	1.288E-05	8.493E-06
0.25	5.030E-08	1.457E-04	1.908E-05	1.661E-05	1.129E-07	1.457E-04	1.528E-05	1.087E-05
0.3	6.339E-07	2.105E-04	2.403E-05	1.841E-05	3.475E-07	2.105E-04	1.953E-05	1.562E-05
0.35	4.128E-07	2.715E-04	2.713E-05	2.136E-05	9.346E-07	2.715E-04	2.435E-05	2.053E-05
0.4	3.134E-07	3.223E-04	2.605E-05	2.174E-05	3.145E-07	3.223E-04	2.833E-05	2.512E-05
0.45	7.816E-07	3.581E-04	2.430E-05	2.454E-05	3.531E-08	3.581E-04	2.842E-05	2.762E-05
0.5	1.070E-07	3.890E-04	1.856E-05	2.195E-05	6.311E-08	3.890E-04	2.729E-05	2.849E-05
0.55	2.030E-07	4.076E-04	1.487E-05	2.009E-05	6.073E-08	4.076E-04	2.555E-05	2.452E-05
0.6	6.517E-07	3.911E-04	1.373E-05	1.531E-05	7.377E-08	3.911E-04	2.546E-05	1.906E-05
0.65	2.623E-07	3.407E-04	1.547E-05	1.306E-05	4.930E-08	3.407E-04	1.726E-05	1.391E-05
0.7	3.408E-07	2.740E-04	1.233E-05	1.005E-05	1.147E-07	2.740E-04	1.204E-05	1.102E-05
0.75	5.650E-08	2.213E-04	1.008E-05	1.004E-05	2.021E-08	2.213E-04	9.210E-06	1.332E-05
0.8	2.904E-07	2.258E-04	9.166E-06	1.047E-05	1.825E-08	2.258E-04	1.020E-05	1.194E-05
0.85	3.924E-07	2.711E-04	1.410E-05	1.356E-05	1.099E-07	2.711E-04	1.339E-05	1.223E-05
0.9	1.588E-07	2.945E-04	1.820E-05	1.706E-05	1.440E-08	2.945E-04	1.708E-05	1.337E-05
0.95	5.847E-07	2.877E-04	1.806E-05	1.426E-05	5.604E-07	2.877E-04	1.570E-05	1.293E-05
1	7.597E-08	2.424E-04	1.143E-05	1.062E-05	8.419E-08	2.424E-04	8.416E-06	7.541E-06

4. Conclusions

Concluding remarks of the presented scheme ANN-PSO-IPA are briefly listed as follows:

- A novel numerical computing method is presented for solving nonlinear biological HIV infection model of latently infected cells using artificial neural network optimized by global capabilities of particle swarm optimization and efficacy of local search with interior-programming algorithm.
- The accuracy of presented scheme is verified by obtaining the overlapping outcomes with the Adams results having accuracy level up to 4–6 decimal places which proves the exactness for the designed scheme.
- The magnitudes of median and semi interquartile range calculated for 100 self-directed executions for a biological nonlinear HIV model that indicate the trustworthiness, steady and accurateness of the algorithm.
- Numerical values listed in the Tables (3-4) and graphical results presented in the figures (2-7) for different performance indices of MAD, RMSE and TIC authenticate the correctness, stability and reliability of the presented scheme.

In future one may exploited the proposed ANN-PSO-IPA as an alternate solver for the solution of potential nonlinear systems [53-60].

Table 4: Statistics based results of Problems 1 for $x(t)$ and $w(t)$

t	$x(t)$				$w(t)$			
	Min	**Max**	**Med**	**SIR**	**Min**	**Max**	**Med**	**SIR**
0	9.421E-08	1.301E-04	6.175E-06	1.030E-05	5.164E-08	1.301E-04	4.158E-06	4.250E-06
0.05	4.070E-08	1.589E-04	1.133E-05	1.555E-05	3.759E-08	1.589E-04	7.579E-06	9.194E-06
0.1	5.235E-08	2.279E-04	9.231E-06	1.404E-05	9.858E-08	2.279E-04	8.595E-06	8.275E-06
0.15	2.757E-08	2.215E-04	1.348E-05	1.372E-05	9.789E-08	2.215E-04	1.579E-05	1.522E-05
0.2	7.820E-07	1.616E-04	1.808E-05	1.286E-05	3.530E-07	1.616E-04	2.277E-05	1.817E-05
0.25	2.741E-07	1.457E-04	2.128E-05	1.488E-05	1.066E-06	1.457E-04	2.576E-05	2.443E-05
0.3	7.716E-07	2.105E-04	2.614E-05	1.637E-05	5.925E-08	2.105E-04	2.364E-05	2.975E-05
0.35	2.699E-07	2.715E-04	2.553E-05	1.442E-05	3.058E-07	2.715E-04	2.241E-05	2.937E-05
0.4	1.796E-07	3.223E-04	1.946E-05	1.608E-05	8.486E-08	3.223E-04	2.012E-05	2.138E-05
0.45	1.073E-07	3.581E-04	1.645E-05	1.803E-05	1.105E-07	3.581E-04	1.677E-05	1.496E-05
0.5	2.976E-08	3.890E-04	1.560E-05	1.612E-05	4.072E-08	3.890E-04	1.542E-05	1.166E-05
0.55	9.826E-08	4.076E-04	1.616E-05	1.606E-05	2.743E-08	4.076E-04	1.579E-05	1.458E-05
0.6	4.456E-08	3.911E-04	1.605E-05	1.441E-05	3.272E-07	3.911E-04	1.621E-05	1.618E-05
0.65	1.348E-07	3.407E-04	1.767E-05	1.548E-05	1.072E-07	3.407E-04	2.314E-05	1.614E-05
0.7	3.462E-07	2.740E-04	2.004E-05	1.229E-05	7.168E-07	2.740E-04	2.655E-05	1.684E-05
0.75	2.145E-07	2.213E-04	1.685E-05	1.397E-05	9.990E-07	2.213E-04	1.886E-05	1.466E-05
0.8	2.705E-08	2.258E-04	1.828E-05	1.671E-05	9.100E-08	2.258E-04	1.548E-05	1.373E-05
0.85	6.305E-07	2.711E-04	1.631E-05	1.796E-05	1.789E-07	2.711E-04	1.919E-05	1.709E-05
0.9	1.322E-07	2.945E-04	1.627E-05	1.598E-05	1.762E-07	2.945E-04	2.308E-05	2.153E-05
0.95	8.401E-07	2.877E-04	1.575E-05	1.348E-05	5.706E-07	2.877E-04	2.414E-05	1.856E-05
1	3.167E-07	2.424E-04	1.499E-05	1.057E-05	2.620E-07	2.424E-04	1.648E-05	1.235E-05

5. Statements:

Funding: This paper has been partially supported by Ministerio de Ciencia, Innovacion y Universidades grant number PGC2018-0971-B-100 and Fundacion Seneca de la Region de Murcia grant number 20783/PI/18.

Conflict of Interest: The authors declare that they have no conflict of interest.

References

[1] Rosenberg, E.S., Altfeld, M., Poon, S.H., Phillips, M.N., Wilkes, B.M., Eldridge, R.L., Robbins, G.K., Richard, T.D., Goulder, P.J. and Walker, B.D., 2000. Immune control of HIV-1 after early treatment of acute infection. Nature, 407(6803), p.523.

[2] Perelson, A.S., 1989. Modeling the interaction of the immune system with HIV. In Mathematical and statistical approaches to AIDS epidemiology (pp. 350-370). Springer, Berlin, Heidelberg.

[3] Perelson, A.S., Kirschner, D.E. and De Boer, R., 1993. Dynamics of HIV infection of CD4+ T cells. Mathematical biosciences, 114(1), pp.81-125.

[4] Ali, N. and Zaman, G., 2016. Asymptotic behavior of HIV-1 epidemic model with infinite distributed intracellular delays. SpringerPlus, 5(1), p.324.

[5] Hattaf, K. and Yousfi, N., 2018. Modeling the adaptive immunity and both modes of transmission in HIV infection. Computation, 6(2), p.37.
[6] Hattaf, K., 2019. Spatiotemporal Dynamics of a Generalized Viral Infection Model with Distributed Delays and CTL Immune Response. Computation, 7(2), p.21.
[7] Wang, L. and Li, M.Y., 2006. Mathematical analysis of the global dynamics of a model for HIV infection of CD4+ T cells. Mathematical Biosciences, 200(1), pp.44-57.
[8] Ali, N., Zaman, G. and Algahtani, O., 2016. Stability analysis of HIV-1 model with multiple delays. Advances in Difference Equations, 2016(1), p.88.
[9] Adomian, G., 1991. Solving frontier problems modelled by nonlinear partial differential equations. Computers & Mathematics with Applications, 22(8), pp.91-94.
[10] Ali, N., Ahmad, S., Aziz, S. and Zaman, G., 2019. The Adomian Decomposition Method for Solving Hiv Infection Model Of Latently Infected Cells. Matrix Science Mathematic (MSMK), 3(1), pp.5-8.
[11] Zibaei, S.A.D.E.G.H. and Namjoo, M.I.E.H.R.A.N., 2015. A nonstandard finite difference scheme for solving fractional-order model of HIV-1 infection of CD4+ t-cells. Iranian Journal of Mathematical Chemistry, 6(2), pp.169-184.
[12] Venkatesh, S.G., Balachandar, S.R., Ayyaswamy, S.K. and Balasubramanian, K., 2016. A new approach for solving a model for HIV infection of CD4+ t-cells arising in mathematical chemistry using wavelets. Journal of Mathematical Chemistry, 54(5), pp.1072-1082.
[13] Prague, M., 2016. Use of dynamical models for treatment optimization in HIV infected patients: a sequential Bayesian analysis approach.
[14] Ghoreishi, M., Ismail, A.M. and Alomari, A.K., 2011. Application of the homotopy analysis method for solving a model for HIV infection of CD4+ T-cells. Mathematical and Computer Modelling, 54(11-12), pp.3007-3015.
[15] Yüzbaşı, Ş., 2012. A numerical approach to solve the model for HIV infection of CD4+ T cells. Applied Mathematical Modelling, 36(12), pp.5876-5890.
[16] Srivastava, V.K., Awasthi, M.K. and Kumar, S., 2014. Numerical approximation for HIV infection of CD4+ T cells mathematical model. Ain Shams Engineering Journal, 5(2), pp.625-629.
[17] Ahmad, I., et al., 2019. Novel applications of intelligent computing paradigms for the analysis of nonlinear reactive transport model of the fluid in soft tissues and microvessels. *Neural Computing and Applications*, *31*(12), pp.9041-9059.
[18] Aidara, S., 2019. Anticipated backward doubly stochastic differential equations with non-Liphschitz coefficients. Applied Mathematics and Nonlinear Sciences, 4(1), pp.9-20.
[19] Yadav, N., Yadav, A., Kumar, M. and Kim, J.H., 2017. An efficient algorithm based on artificial neural networks and particle swarm optimization for solution of nonlinear Troesch's problem. Neural Computing and Applications, 28(1), pp.171-178.
[20] Fateh, M.F., et al., 2019. Differential evolution based computation intelligence solver for elliptic partial differential equations. *Frontiers of Information Technology & Electronic Engineering*, *20*(10), pp.1445-1456.
[21] Mehmood, A., et al., 2019. Integrated intelligent computing paradigm for the dynamics of micropolar fluid flow with heat transfer in a permeable walled channel. *Applied Soft Computing*, *79*, pp.139-162.
[22] Umar, M., Sabir, Z. and Raja, M.A.Z., 2019. Intelligent computing for numerical treatment of nonlinear prey–predator models. Applied Soft Computing, 80, pp.506-524.

[23] Raja, M.A.Z., Shah, F.H., Tariq, M. and Ahmad, I., 2018. Design of artificial neural network models optimized with sequential quadratic programming to study the dynamics of nonlinear Troesch's problem arising in plasma physics. Neural Computing and Applications, 29(6), pp.83-109.

[24] Schaff, J.C., Gao, F., Li, Y., Novak, I.L. and Slepchenko, B.M., 2016. Numerical approach to spatial deterministic-stochastic models arising in cell biology. PLoS computational biology, 12(12), p.e1005236.

[25] Momani, S., Abo-Hammour, Z.S. and Alsmadi, O.M., 2016. Solution of inverse kinematics problem using genetic algorithms. Applied Mathematics & Information Sciences, 10(1), p.225.

[26] Raja, M.A.Z., Khan, J.A. and Haroon, T., 2015. Stochastic numerical treatment for thin film flow of third grade fluid using unsupervised neural networks. Journal of the Taiwan Institute of Chemical Engineers, 48, pp.26-39.

[27] Soize, C., 2012. Stochastic models of uncertainties in computational structural dynamics and structural acoustics. In Nondeterministic Mechanics (pp. 61-113). Springer, Vienna.

[28] Pelletier, F., Masson, C. and Tahan, A., 2016. Wind turbine power curve modelling using artificial neural network. Renewable Energy, 89, pp.207-214.

[29] Effati, S. and Pakdaman, M., 2010. Artificial neural network approach for solving fuzzy differential equations. Information Sciences, 180(8), pp.1434-1457.

[30] Raja, M.A.Z., Farooq, U., Chaudhary, N.I. and Wazwaz, A.M., 2016. Stochastic numerical solver for nanofluidic problems containing multi-walled carbon nanotubes. Applied Soft Computing, 38, pp.561-586.

[31] Sabir, Z., Manzar, M.A., Raja, M.A.Z., Sheraz, M. and Wazwaz, A.M., 2018. Neuro-heuristics for nonlinear singular Thomas-Fermi systems. Applied Soft Computing, 65, pp.152-169.

[32] Raja, M.A.Z., Mehmood, J., Sabir, Z., Nasab, A.K. and Manzar, M.A., 2019. Numerical solution of doubly singular nonlinear systems using neural networks-based integrated intelligent computing. Neural Computing and Applications, 31(3), pp.793-812.

[33] Raja, M.A.Z., Umar, M., Sabir, Z., Khan, J.A. and Baleanu, D., 2018. A new stochastic computing paradigm for the dynamics of nonlinear singular heat conduction model of the human head. The European Physical Journal Plus, 133(9), p.364.

[34] Zhang, Z., El-Moselhy, T.A., Elfadel, I.M. and Daniel, L., 2013. Stochastic testing method for transistor-level uncertainty quantification based on generalized polynomial chaos. IEEE Transactions on Computer-Aided Design of Integrated Circuits and Systems, 32(10), pp.1533-1545.

[35] He, W., Chen, Y. and Yin, Z., 2015. Adaptive neural network control of an uncertain robot with full-state constraints. IEEE transactions on cybernetics, 46(3), pp.620-629.

[36] Zameer, A., et al., 2017. Intelligent and robust prediction of short term wind power using genetic programming based ensemble of neural networks. *Energy conversion and management*, *134*, pp.361-372.

[37] Shi, Y. and Eberhart, R. C., 1999. Empirical study of particle swarm optimization. In Proceedings of the 1999 Congress on Evolutionary Computation-CEC99 (Cat. No. 99TH8406) (Vol. 3, pp. 1945-1950). IEEE.

[38] Engelbrecht, A. P., 2007. Computational intelligence: an introduction. John Wiley & Sons.

[39] Zameer, A., et al., 2020. Fractional-order particle swarm based multi-objective PWR core loading pattern optimization. *Annals of Nuclear Energy*, *135*, p.106982.

[40] Raja, M.A.Z., 2014. Solution of the one-dimensional Bratu equation arising in the fuel ignition model using ANN optimised with PSO and SQP. *Connection Science*, *26*(3), pp.195-214.
[41] Khare, A. and Rangnekar, S., 2013. A review of particle swarm optimization and its applications in solar photovoltaic system. Applied Soft Computing, 13(5), pp.2997-3006.
[42] Esmin, A. A., Coelho, R. A. and Matwin, S., 2015. A review on particle swarm optimization algorithm and its variants to clustering high-dimensional data. Artificial Intelligence Review, 44(1), pp.23-45.
[43] Brzeziński, D.W., 2017. Comparison of fractional order derivatives computational accuracy-right hand vs left hand definition. Applied Mathematics and Nonlinear Sciences, 2(1), pp.237-248.
[44] Youssef, I.K. and El Dewaik, M.H., 2017. Solving Poisson's Equations with fractional order using Haarwavelet. Applied Mathematics and Nonlinear Sciences, 2(1), pp.271-284.
[45] Al-Ghafri, K.S. and Rezazadeh, H., 2019. Solitons and other solutions of (3+ 1)-dimensional space–time fractional modified KdV–Zakharov–Kuznetsov equation. Applied Mathematics and Nonlinear Sciences, 4(2), pp.289-304.
[46] Hattaf, K. and Yousfi, N., 2016. Global properties of a discrete viral infection model with general incidence rate. Mathematical Methods in the Applied Sciences, 39(5), pp.998-1004.
[47] Hattaf, K. and Yousfi, N., 2016. A numerical method for a delayed viral infection model with general incidence rate. Journal of King Saud University-Science, 28(4), pp.368-374.
[48] Raja, M.A.Z., Aslam, M.S., Chaudhary, N.I. and Khan, W.U., 2018. Bio-inspired heuristics hybrid with interior-point method for active noise control systems without identification of secondary path. *Frontiers of Information Technology & Electronic Engineering*, *19*(2), pp.246-259.
[49] Stefanova, M., Yakunin, S., Petukhova, M., Lupuleac, S. and Kokkolaras, M., 2018. An interior-point method-based solver for simulation of aircraft parts riveting. Engineering Optimization, 50(5), pp.781-796.
[50] Bleyer, J., 2018. Advances in the simulation of viscoplastic fluid flows using interior-point methods. Computer Methods in Applied Mechanics and Engineering, 330, pp.368-394.
[51] Raja, M.A.Z., Ahmed, U., Zameer, A., Kiani, A.K. and Chaudhary, N.I., 2019. Bio-inspired heuristics hybrid with sequential quadratic programming and interior-point methods for reliable treatment of economic load dispatch problem. Neural Computing and Applications, 31(1), pp.447-475.
[52] Mangoni, D., Tasora, A. and Garziera, R., 2018. A primal–dual predictor–corrector interior point method for non-smooth contact dynamics. Computer Methods in Applied Mechanics and Engineering, 330, pp.351-367.
[53] Yokuş, A. and Gülbahar, S., 2019. Numerical Solutions with Linearization Techniques of the Fractional Harry Dym Equation. Applied Mathematics and Nonlinear Sciences, 4(1), pp.35-42.
[54] Brzeziński, D.W., 2018. Review of numerical methods for NumILPT with computational accuracy assessment for fractional calculus. Applied Mathematics and Nonlinear Sciences, 3(2), pp.487-502.
[55] Yokuş, A., 2018. Comparison of Caputo and conformable derivatives for time-fractional Korteweg–de Vries equation via the finite difference method. International Journal of Modern Physics B, 32(29), p.1850365.

[56] Yokus, A., 2018. Numerical solution for space and time fractional order Burger type equation. Alexandria engineering journal, 57(3), pp.2085-2091.
[57] Mehmood, A., et al., 2019. Backtracking search heuristics for identification of electrical muscle stimulation models using Hammerstein structure. *Applied Soft Computing*, *84*, p.105705.
[58] Akbar, S., et al., 2019. Novel application of FO-DPSO for 2-D parameter estimation of electromagnetic plane waves. *Neural Computing and Applications*, *31*(8), pp.3681-3690.
[59] Raja, M.A.Z., Aslam, M.S., Chaudhary, N.I., Nawaz, M. and Shah, S.M., 2019. Design of hybrid nature-inspired heuristics with application to active noise control systems. *Neural Computing and Applications*, *31*(7), pp.2563-2591.
[60] Zameer, A., Majeed, M., Mirza, S.M., Raja, M.A.Z., Khan, A. and Mirza, N.M., 2019. Bio-inspired heuristics for layer thickness optimization in multilayer piezoelectric transducer for broadband structures. *Soft Computing*, *23*(10), pp.3449-3463.